

Lamellar Macular Hole: A Clinicopathologic Correlation of Surgically Excised Epiretinal Membranes

Barbara Parolini,^{1,2} Ricarda G. Schumann,^{2,3} Matteo G. Cereda,¹ Christos Haritoglou,³ and Grazia Pertile¹

PURPOSE. To correlate clinical and optical coherence tomographic (OCT) features with morphologic and immunohistochemical findings of epiretinal membranes (ERMs) in lamellar macular holes (LMHs).

METHODS. Nineteen specimens were removed from 19 eyes during vitrectomy for lamellar macular hole with ERM and internal limiting membrane peeling, and were processed for transmission electron microscopy and immunohistochemistry by cross-sectional and flat-mount preparation techniques. By using OCT criteria and intraoperative observations, ERM specimens were divided into two groups: 13 “dense” and 6 “tractional” membranes. Patients’ records were reviewed.

RESULTS. “Dense” ERMs were seen with abundant clusters of fibrous long-spacing collagen embedded in compactly folded native vitreous collagen strands. Posterior hyaloids were attached to the retina in the majority of cases. Both groups of ERMs showed positive immunoreactivity for glial fibrillar acidic protein and hyalocyte markers. Anti- α -smooth muscle actin labeling was most positive in “tractional” ERMs. Surgery resulted in significant improvement (74%) of visual acuity, with a mean gain of 2 Snellen lines in both groups. All other patients (26%) preserved vision. Three patients (16%) developed a full-thickness macular defect requiring additional surgery.

CONCLUSIONS. Morphologic components differ in epiretinal cell proliferations of LMHs. In association with degradation of vitreous collagen, glial cells and hyalocytes seem to play an important role in LMH development. Since functional benefit after surgery was limited and progression to a full-thickness macular defect was a notable complication, we recommend caution in proceeding with surgical intervention. Further investigations are needed to elucidate whether “dense” and “tractional” LMHs represent different disease entities or different stages of one disorder. (*Invest Ophthalmol Vis Sci.* 2011;52:9074–9083) DOI:10.1167/iov.11-8227

The accuracy of lamellar macular hole (LMH) diagnosis was strongly improved by the introduction of optical coherence tomography (OCT), although our understanding of pathogenesis, clinical progression, and therapy of this macular defect remains incomplete.

From the ¹Department of Ophthalmology, Ospedale Sacrocuore Don Calabria, Negrar, Verona, Italy; and the ²Department of Ophthalmology, Ludwig-Maximilians-University, Munich, Germany.

³These authors contributed equally to the work presented here and should therefore be regarded as equivalent authors.

Submitted for publication July 15, 2011; revised September 16, 2011; accepted October 13, 2011.

Disclosure: **B. Parolini**, None; **R.G. Schumann**, None; **M.G. Cereda**, None; **C. Haritoglou**, None; **G. Pertile**, None

Corresponding author: Ricarda G. Schumann, Ludwig-Maximilians-University, Department of Ophthalmology, Mathildenstrasse 8, D-80336 Munich, Germany; ricarda.schumann@med.uni-muenchen.de.

Although progress was made in visualizing retinal anatomy by OCT during the last decade, there is no generally accepted definition of LMH. To distinguish LMHs from other similar macular lesions, such as macular pseudoholes, Witkin and colleagues¹ recently proposed distinct OCT criteria based on qualitative image analysis without measurement of retinal thickness. According to these four criteria, diagnosis of a lamellar macular hole is based on: (1) an irregular foveal contour; (2) a break in the inner fovea; (3) a dehiscence of the inner foveal retina from the outer retina; and (4) an absence of a full-thickness foveal defect with intact foveal photoreceptors.

By biomicroscopic and fluorescein angiographic findings, lamellar macular holes were initially described to result from cystoid macular edema.² Recent findings of OCT studies indicate that LMHs may result from vitreoretinal traction representing an abortive process in full-thickness macular hole formation.^{3–6} Since epiretinal membranes (ERMs) are a common finding reported in the majority of eyes with lamellar macular holes, pathogenesis, configuration, and progression of LMHs are believed to be influenced or even caused by tangential retinal traction due to ERM contraction.^{1,4,7,8}

However, different appearances of ERMs were observed by ultrahigh-resolution OCT.¹ First, ERMs were demonstrated as a thin highly reflective line anteriorly situated but separated from the retinal nerve fiber layer (RNFL) corresponding to previously reported ERMs on OCT. Second, unusual appearing ERMs presented as a highly reflective line with a moderately reflective material filling the space between the inner border of the ERM and the RNFL. Although ERMs with unusual appearance were frequently seen in eyes with LMHs, the morphologic correlate is unknown.

Unusual appearing ERMs can be surgically removed during vitrectomy. According to our intraoperative observations, this specific epiretinal tissue has a yellow dense appearance and a fluffy consistency, and could be classified neither as vitreous cortex nor as regular ERM. It can be completely separated from the retina and the internal limiting membrane (ILM). Intraoperatively, LMHs with unusual ERM mostly show no sign of tangential or anteroposterior traction.

Based on these observations made during surgery, the aim of this study was to define the morphologic correlate of two distinct groups of epiretinal membranes in LMHs: “dense” ERMs, presenting with an unusual appearance but no signs of traction as described earlier; and “tractional ERMs,” presenting as typical epiretinal tissue in OCT and during vitreoretinal surgery that exert tangential traction at the retina. Furthermore, this study was conducted to correlate clinical and tomographic features with morphologic and immunohistochemical findings within these two groups of ERMs, and to report on our results of surgical intervention in LMHs, thereby identifying implications for macular surgery.

MATERIALS AND METHODS

From a series of surgically excised ERM and ILM specimens removed during surgery for lamellar macular hole between January 2008 and June 2010, 19 specimens were processed for light and transmission electron microscopy as well as immunohistochemistry. The specimens were obtained from 19 eyes of 19 patients that were diagnosed with lamellar macular holes at OCT (Spectralis-OCT; Heidelberg Engineering, Heidelberg, Germany). Exclusively, specimens from patients with LMH presenting with epiretinal tissue were included in this study. Recommendation of vitrectomy with ERM/ILM peeling was based on three variable settings: progression of clinical data, such as significant decrease in visual acuity during preoperative follow-up period and/or significant impairment and decrease of quality of daily life; association with a decrease in foveal thickness and/or an increase of LMH diameter; and the presence of ERM and/or complaining of metamorphopsia. Eight patients were male and 11 patients were female, ranging in age from 50 to 82 years, with a mean of 72 years. The refractive error ranged between +2.00 and -8.00 sphere. Table 1 shows the main clinical data of all patients. Patients were examined preoperatively, 1 week as well as 1, 3, and 6 months postoperatively. The OCT characteristics that lead to the diagnosis of a lamellar macular hole were proposed by Witkin and colleagues¹ as follows: (1) an irregular foveal contour; (2) a break into the inner fovea; (3) a separation of the inner from the outer retinal layer, leading to intraretinal splitting; and (4) the absence of a full-thickness foveal defect with an intact photoreceptor layer posterior to the area of foveal dehiscence.

The ERM was classified at OCT as “tractional” when a thin hyperreflective line was observed immediately anterior and separate from the RNFL (Fig. 1A). The ERM was classified at OCT as “dense” when hyporeflective material filled the space between the inner border of the ERM and RNFL (Fig. 1B).

By means of OCT, a series of preoperative features were analyzed as follows: the integrity of the outer nuclear layer (ONL); the presence of outer foveal hyporeflective defects, which are focal disruptions or interruptions in the normal hyperreflective inner segment-outer seg-

ment (IS-OS) junction; abnormality of the external limiting membrane (ELM) and the presence of a hyperreflective line on the innermost layer of the retina. By means of infrared imaging (Spectralis-OCT; Heidelberg Engineering), we also analyzed the visibility of retinal folds in the macular area. Best-corrected visual acuity (BCVA) and the presence of metamorphopsia were recorded at each visit. No other ocular pathologies coexisted in the patients.

Surgical Procedure

All patients underwent a standard pars plana vitrectomy. The presence of posterior vitreous detachment (PVD) was recorded intraoperatively. PVD was induced, when necessary, by suction with the vitrectomy probe around the optic nerve head. The posterior hyaloid was detached from the retina and PVD was extended to the periphery. ERM and ILM were peeled sequentially without vital dye, being the ERM on top and separate from the ILM. Figure 2A shows the unusual appearance of a “dense” ERM during surgery, presenting as yellow dense tissue with a fluffy consistency. In contrast, Figure 2B shows a typical appearing “tractional” ERM, presenting more transparent and easy to grasp in bigger flaps during vitrectomy. After peeling, vitrectomy was extended to the periphery. Air was used to fill the vitreous cavity as a final tamponade through a fluid-air exchange. No face-down positioning was recommended. This study was approved by the Institutional Review Board and the Ethics Committee. Informed consent was obtained from all patients, in accordance with the tenets of the Declaration of Helsinki.

Specimen Preparation

The excised ERM and ILM specimens were immediately placed into a mixture of 2% paraformaldehyde and 0.1% glutaraldehyde in 0.1 M PBS (pH 7.4). Total amounts of 28 specimens were removed from 19 eyes of 19 patients that were then sent masked to the Department of Ophthalmology at the Ludwig-Maximilians-University Munich for further preparation, photodocumentation, and analysis.

TABLE 1. Clinical Data and OCT Characteristics of Patients with Lamellar Macular Holes

Factor	Sex/ Age (y)	Type of LMH According to ERM	OCT Characteristics		Preop. BCVA in logMAR	Postop. BCVA in logMAR	Metamorphopsia	State of Posterior Hyaloid	Preop. State of the Lens
			Splitting Location	State of ELM					
1	M/81	Dense	OPL-ONL	Defect	0.4	0.4†	-	A	Phakic
2	F/79	Dense	OPL-ONL	Integrity	0.4	0.0	-	A	IOL
3	M/76	Dense	OPL-ONL	n.a.	1.0	0.0	-	A	Phakic
4	M/71	Dense	OPL-ONL	Defect	0.3	0.0	-	A	IOL
5	F/72	Dense	OPL-ONL	Defect	0.2	0.1	-	A	IOL
6	M/70	Dense	OPL-ONL	Defect	0.2	0.0	-	PVD	IOL
7	M/82	Dense	OPL-ONL	Defect	0.4	0.1	-	A	Phakic
8	F/73	Dense‡	OPL-ONL	Defect	0.5	0.5†	-	A	Phakic
9	M/74	Dense	OPL-ONL	Defect	0.5	0.0	-	PVD	IOL
10	M/72	Dense‡	OPL-ONL	Defect	0.3	0.3†	-	PVD	Phakic
11	M/72	Dense	OPL	Defect	0.7	0.7	-	A	IOL
12	F/59	Dense	n.a.	n.a.	0.3	0.2	-	n.a.	IOL
13	F/80	Dense	OPL-ONL	n.a.	0.1	0.1	-	A	Phakic
14	F/74	Tractional	OPL	Integrity	0.5	0.4	+	A	Phakic
15	F/80	Tractional	OPL	Integrity	0.5	0.4	-	A	Phakic
16	F/50	Tractional	OPL	Integrity	0.2	0.0	+	A	Phakic
17	F/61	Tractional	OPL	Integrity	0.2	n.a.	-	n.a.	Phakic
18	F/59	Tractional	OPL	Integrity	0.3	0.0	+	A	Phakic
19	M/82	Tractional	OPL	Integrity	0.7	0.5	+	n.a.	IOL

M, male; F, female; A, attached posterior vitreous; PVD, complete posterior vitreous detachment; n.a., not applicable.

* All patients with phakic eyes at the time of surgery underwent combined vitrectomy with phacoemulsification and IOL implantation for the presence of cataract.

† Postoperative progression to full-thickness macular hole.

‡ Associated with extrafoveal epiretinal tissue.

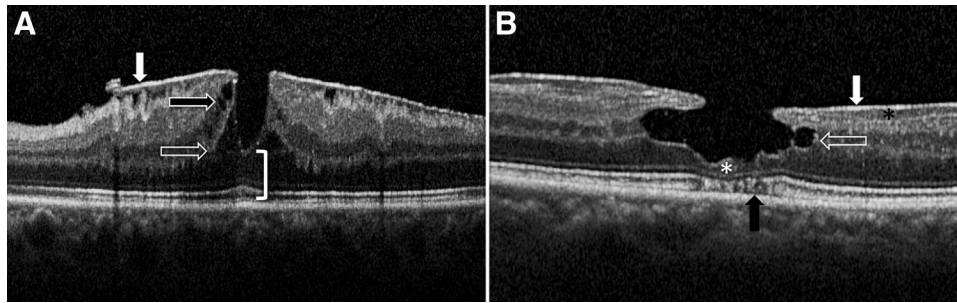


FIGURE 1. Preoperative OCT findings. **(A)** OCT image of a 61-year-old female presenting with LMH associated with a “tractional” epiretinal membrane. The ERM is directly visible on top of the RNFL as a hyperreflective line (*white arrow*). OCT image demonstrates that the intraretinal split is both at the level of the outer plexiform layer (OPL, *white empty arrow*) and the inner nuclear layer (INL, *black arrow with white outline*). The outer nuclear layer (ONL, *square bracket*) is not split. The external limiting membrane (ELM) and the inner segment-outer segment (IS-OS) junction are preserved. **(B)** OCT image of an 82-year-old male presenting with LMH associated with a “dense” epiretinal membrane. Hyporeflective material (*black asterisk*) fills the space between the ERM (*white arrow*) and the RNFL. The intraretinal split is at the level of the OPL (*white empty arrow*) and the ONL (*white asterisk*). The IS-OS junction shows an altered profile (*black arrow*).

For immunohistochemistry, specimens of 11 patients were dehydrated in graded concentrations of ethanol and embedded using a commercial embedding kit (Lowicryl K4M; Polysciences Europe GmbH, Eppelheim, Germany). Semithin sections of 400 to 600 nm were stained with an aqueous mixture of 1% toluidine blue and 2% sodium borax. Immunohistochemical staining was performed on semithin sections (Lowicryl resin) mounted on glass slides as described previously.⁹ Primary antibodies were used for glial and retinal cells (anti-glial fibrillar acidic protein [anti-GFAP]; DAKO, Hamburg, Germany; anti- α -Smooth muscle actin [anti- α -SMA]; Sigma-Aldrich, Taufkirchen, Germany; anti-cellular retinaldehyde binding protein [anti-CRALBP]; Santa Cruz Biotechnology, Heidelberg, Germany; anti-neurofilament [anti-NF]; DAKO), for hyalocytes (anti-CD45; Santa Cruz Biotechnology), and for macrophages (anti-CD 68; Santa Cruz Biotechnology) as listed in Table 2. Primary antibodies were diluted according to the manufacturer's instructions. The second antibodies (donkey anti-mouse CY3, donkey anti-rabbit CY2, donkey anti-goat CY5; Dianova, Hamburg, Germany) were added together, each in 1:100 phosphonobutane tricarboxylic acid. Antifading mounting medium 4',6'-diamidino-2-phenylindol (DAPI, AKS-38448; Dianova) was used for cell nuclei staining. We used labeling combinations of three antibodies because the maximum number of fluochromes used at one time was limited, and the antibody combinations were limited as a result of the species from which they were originating. Sections were analyzed using a fluorescence microscope (DM 2500; Leica, Wetzlar, Germany). For conventional light microscopy, specimen sections were stained

with an aqueous mixture of 1% toluidine blue and 2% sodium borax. For photodocumentation, we used a digital camera to image the specimens at magnifications between $\times 50$ and $\times 400$ (ProgRes CF; Jenoptik, Jena, Germany).

In four cases, specimens were prepared as whole flat mounts after fixation. Under a stereomicroscope (MS 5; Leica), the specimens were placed onto glass slides. To show the maximum area of their surface, specimens were unfolded using glass pipettes. Indirect immunocytochemistry was performed on flat-mounted specimens according to the procedure described earlier using anti-GFAP, anti- α -SMA, and anti-CD45 as primary antibodies. For negative control, primary antibodies were substituted with diluents, followed by incubation with secondary antibody alone. All other procedures were identical with normal immunolabeling. Antifading mounting medium DAPI was applied for cell nuclei staining, and a cover slide was added.

To specify the ultrastructural features of epiretinal tissue specimens in detail, transmission electron microscopy was performed in four cases. After fixation, specimens were processed for postfixation with osmium tetroxide 2% (Dalton's fixative), followed by dehydration in graded series of ethanol and embedding in epoxy resin (Epon 812). Ultrathin sections of 60 nm were contrasted with uranyl acetate and lead citrate. Analysis and imaging were performed using a light microscope (Zeiss, Jena, Germany) and an electron microscope (EM 9 S-2; Zeiss). Measurement of collagen fibrils and their analysis were performed using a commercial imaging/editing software program and

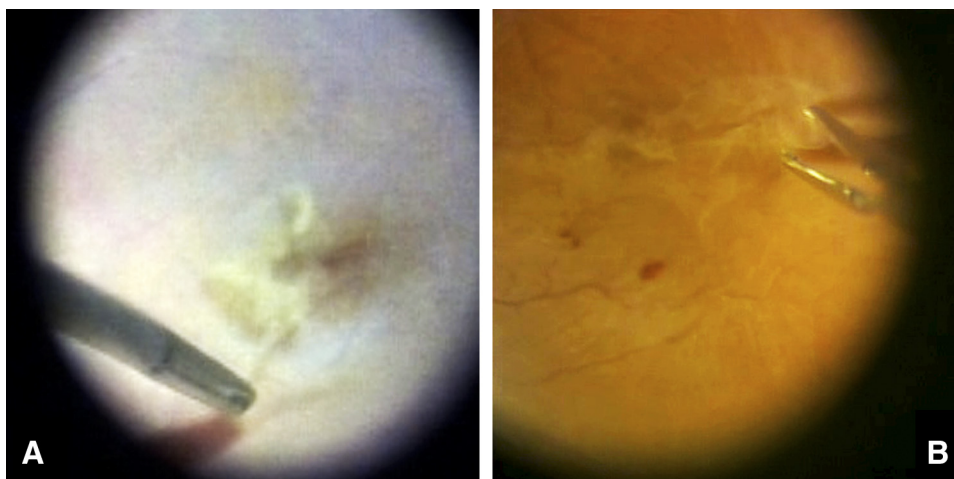


FIGURE 2. Intraoperative appearance of epiretinal tissue. **(A)** Intraoperative view of the epiretinal tissue classified as “dense” membrane during the peeling phase. This specific epiretinal tissue has a yellow dense appearance and a fluffy consistency, and was macroscopically classified as neither vitreous cortex nor regular epiretinal membrane. **(B)** Intraoperative view of the epiretinal tissue classified as “tractional” membrane during the peeling phase. The tissue is transparent, consistent, and easier to separate from the retina as one sheet. The shining of the vitreoretinal surface is easily visible.

TABLE 2. Antibodies Used for Immunohistochemical Staining

Anti-	Target Structure
Glial fibrillic acidic protein (GRAP)	Intermediate-type filaments of glial cells
Cellular retinaldehyde binding protein (CRALBP)	Glial cells and retina pigment epithelial cells
Neurofilament (NF)	Retinal ganglion cells
alpha Smooth muscle actin (α -SMA)	Intracellular actin filaments
CD45	Hyalocytes
CD64	Hyalocytes
CD68	Macrophages/Microglia

analytical software (Adobe Photoshop CS4; Adobe, San Jose, CA; and SPSS 18.0; SPSS Inc., Chicago, IL, respectively).

RESULTS

Clinical Data of Patients

The preoperative OCT morphologic analysis made it possible to observe 13 “dense” membranes and 6 “tractional” membranes. In two eyes with “dense” membranes, an extrafoveal tractional epiretinal membrane was coexisting. Postoperatively data were available for 18 eyes, since one patient was lost to follow-up. Clinical data and OCT characteristics are presented in Table 1.

As demonstrated in Figure 3 and Table 1, “tractional” membranes were observed with integrity of the ONL and the ELM, with a normal hyperreflective IS-OS junction. The intraretinal split in “tractional” membranes was in the OPL. The intraretinal split in “dense” membranes was in the OPL, but penetrated into the ONL. “Dense” membranes presented alterations of the ONL, disruption of the ELM, and hyporeflective defects with focal interruption of the IS-OS junction. A hyperreflective line in the innermost layer of the retina was visible in all eyes with any type of ERM.

The infrared image showed that retinal folds were always present in “tractional” membranes. In the two “dense” mem-

branes associated with extrafoveal epiretinal tissue, retinal folds were visible only where extrafoveal membranes were located. Retinal folds were absent in all other “dense” membranes.

Eight patients were already pseudophakic at the time of surgery (seven patients with “dense” and one patient with “tractional” membranes). All other patients underwent combined vitrectomy with phacoemulsification and intraocular lens implantation for cataract formation. Only four patients with “tractional” membranes and none with “dense” membranes complained of metamorphopsia.

Intraoperatively, the vitreous was actively detached from the posterior pole in nine eyes with “dense” membranes, and in four eyes with “tractional” membranes. A complete PVD was present in three eyes with “dense” membranes only. The status of the vitreous was not recorded in three patients (one eye with “dense” and two eyes with “tractional” membranes).

After surgery, the retinal architecture improved in all patients except for three patients (16%) that developed a full macular defect. The retinal profile was more regular than the preoperative profile in both “dense” and “tractional” membranes, resulting in the disappearance of the intraretinal split and in restored continuity of the ONL and the inner retinal layers (Fig. 3). However, in “dense” membranes some alterations of the outer layers could still be visible.

FIGURE 3. Pre- and postoperative OCT findings of two patients. (A, C, E) OCT images of a 59-year-old female with LMH associated with a “tractional” epiretinal membrane. (B, D, F) OCT images of a 74-year-old male with LMH associated with a “dense” epiretinal membrane. (A) Preoperative OCT findings: “Tractional” membrane (*white arrow*) presents integrity of the ONL and the ELM with an unremarkable hyperreflective IS-OS junction (*square bracket*). Intraretinal split is seen at the level of the OPL (*empty white arrow*). (B) Preoperative OCT findings: “Dense” membrane (*asterisk*) shows location of the intraretinal split at the OPL (*empty white arrow*) penetrating into the ONL. There, hyporeflective defects with focal interruption of the IS-OS junction are visible (*black arrow with white outline*). (C) One month after surgery: The inner retinal layers are not split but there are cystic spaces in the INL and the OPL (*white dot*). ONL and outer segments are preserved (*square bracket*). (D) One month after surgery: The intraretinal split is not visible; however, there is no continuity of the ONL. Some hyporeflective defects of the IS-OS are still visible (*black arrow with white outline*). (E) Six months after surgery: The inner retinal layers are not split and the cystic spaces have disappeared. ONL and outer segments are well preserved (*square bracket*). (F) Six months after surgery: The inner profile is more regular; however, there is no complete continuity of the ONL and the IS-OS junction (*black arrow with white outline*).

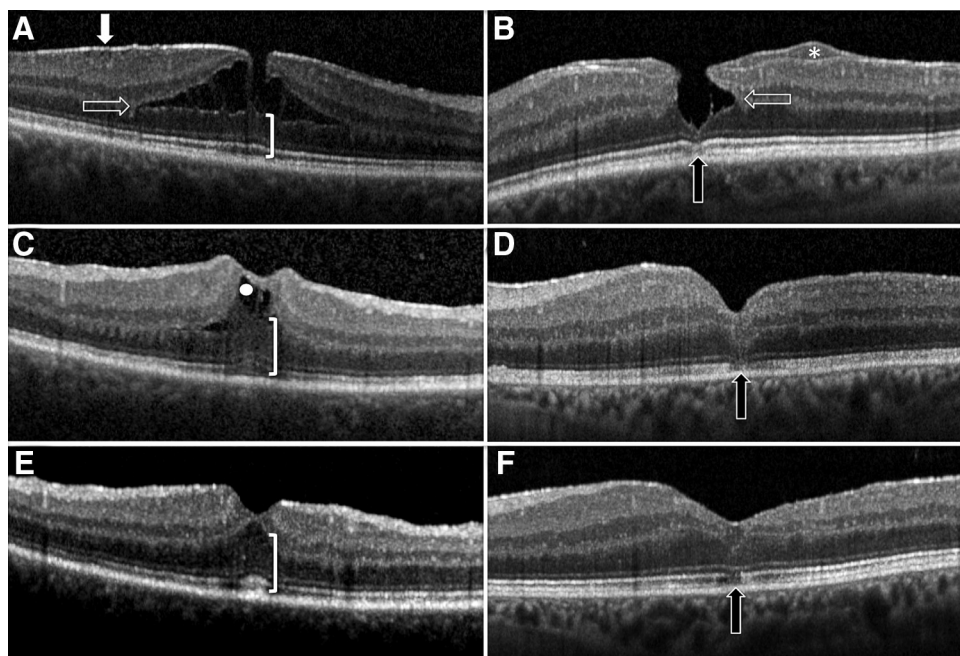


TABLE 3. Morphologic Features of Epiretinal Membranes Removed for Lamellar Macular Holes

Morphologic Feature	Number of Patients* (<i>n</i> = 15) Presenting Morphologic Features in Sectioned Epiretinal Tissue Specimens		
	"Dense" Membrane (<i>n</i> = 10)	"Tractional" Membrane (<i>n</i> = 5)	Total
Internal limiting membrane	6	3	9
Epiretinal cell proliferation	10	5	15
Masses of collagen matrix	10	5	15

* Including specimens prepared by cross-sectioning procedures (*n* = 15), excluding specimens prepared by flat-mount procedure (*n* = 3).

Pre- and postoperative logMAR BCVA improved significantly in patients with LMHs after vitrectomy with ILM/ERM peeling (Wilcoxon test, $P = 0.01$). Pre- and postoperative logMAR BCVA in the "dense" group was 0.4 ± 0.2 (average \pm SD) and 0.2 ± 0.2 , respectively. The difference was statistically significant (Wilcoxon test, $P = 0.012$). Pre- and postoperative logMAR BCVA in the "tractional" group was 0.4 ± 0.2 (average \pm SD) and 0.2 ± 0.3 , respectively. The difference was also statistically significant (Wilcoxon test, $P = 0.041$). Postoperative BCVA was recorded after 12 ± 2 months (average \pm SD).

In this study, we found a mean gain of 2.1 Snellen lines. The improvement of visual acuity was statistically significant in patients with both "dense" and "tractional" membranes. Only five of our patients were found with unchanged vision. All other patients were found with improved visual acuity. None of our patients experienced deterioration of vision. Three patients with a "dense" membrane were diagnosed with a full-thickness macular hole at the first postoperative week. These patients were managed with fluid-gas exchange using sulfur hexafluoride as tamponade at 20% dilu-

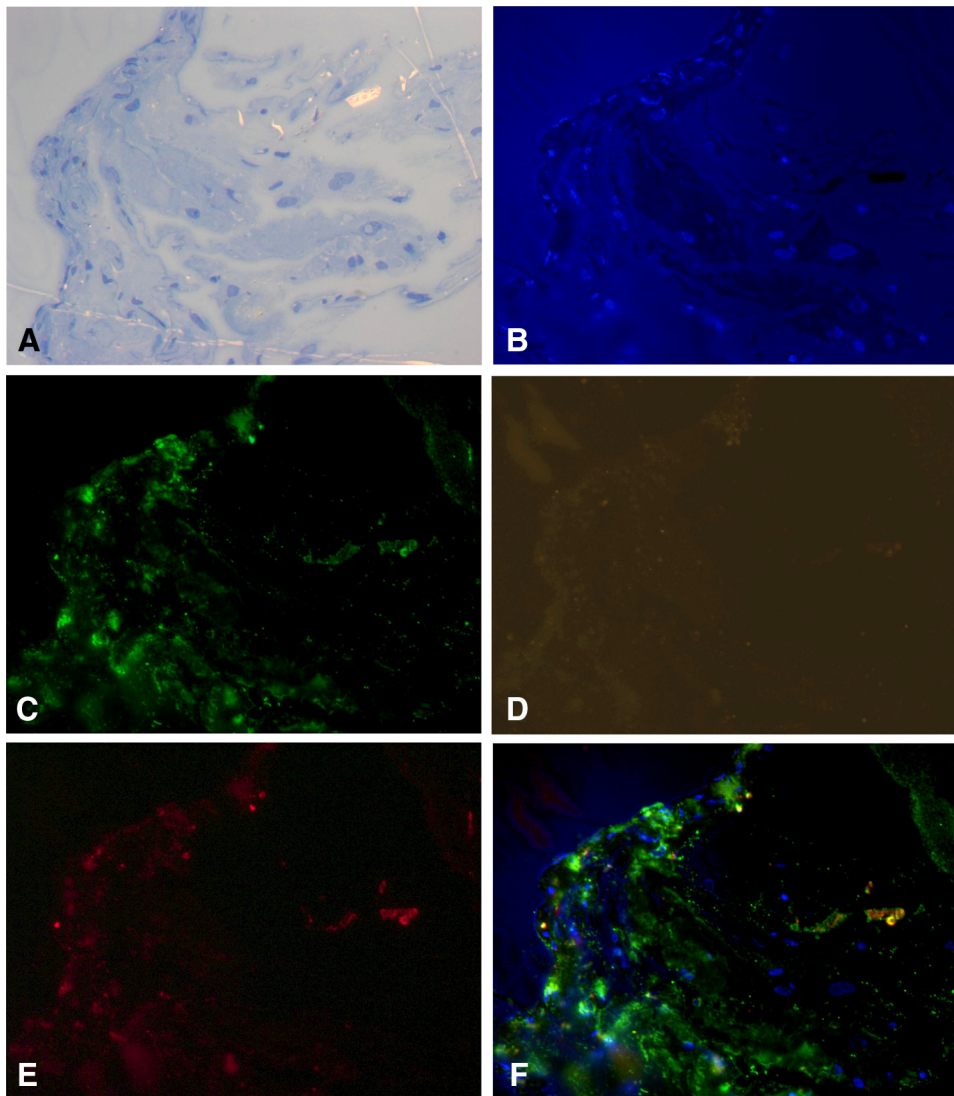


FIGURE 4. Morphologic and immunohistochemical findings of epiretinal tissue with characteristic yellow dense appearance removed for lamellar macular hole with "dense" ERM. (A–F) Sections (Lowicryl Embedding Kit) of the same detail of one specimen. (A) Light micrograph with toluidine blue staining shows a compact and multiply folded membrane composed of cellular proliferation embedded in abundant extracellular matrix. The ILM is not demonstrated. (B) Antifading mounting medium DAPI was used for cell nuclei staining (blue). (C) Indirect immunofluorescence staining with anti-GFAP (green) was positive in all tested specimens. (D) The hyalocyte cell marker anti-CD45 was negative tested in this specimen but inconsistent positive in others. (E) A sparse positive staining with anti-CD64, a hyalocyte cell marker, is demonstrated, and (F) shown to be colocalized with anti-GFAP (yellow) as presented in this merged immunofluorescence micrograph. Original magnification: $\times 400$.

tion, and with face-down positioning. The macular holes closed successfully.

Morphologic Features

Morphologic structures were analyzed in all cross-sectioned specimens ($n = 15$), including embedded specimens (in Lowicryl) for further immunocytochemical staining ($n = 11$), and embedded specimens (in Epon) for further transmission electron microscopy ($n = 4$) (Table 3). Flat-mounted specimens were excluded from this morphologic analysis because flat-mount preparation made it impossible to perform topographical description of morphologic components ($n = 4$).

Light microscopy revealed that cell proliferation and collagen matrix were present in epiretinal tissue of all eyes with lamellar macular holes. The ILM was seen in 60% of cases in both groups, in “dense” and “tractional” membranes. In 40% of cases, ILM specimens could not be collected after peeling or were lost during the preparation procedure due to their small size and translucent appearance. Analyzing the presence of epiretinal cell proliferation and the presence of collagen, it was similar in the two groups. However, the collagen matrix showed different appearances in a comparison of both groups. “Dense” membranes were shown as compact tissue, with relatively few cells embedded in masses of collagen. The collagen

matrix was sorted as broad strands multiply and closely folded (Fig. 4A).

In contrast, “tractional” membranes presented with basal lamina-like collagen strands less folded with multilayered thin cytoplasmic cell processes often situated along one side of the collagen strand (Figs. 5A, 5B). If the ILM was seen, it could be clearly distinguished from collagen strands by its typical undulated retinal side and the smooth vitreal side at higher magnifications. Mostly, the ILM was found blank or with single cells attached to the vitreal side (Fig. 5A).

Transmission electron microscopy of “dense” membranes demonstrated collagen strands in higher magnification and allowed characterization of native vitreous collagen, which was the major type of collagen observed (Fig. 6A). Newly formed collagen, however, was also found in all specimens. Collagen strands of “dense” membranes enclosed abundant clusters of compact fibrous long-spacing collagen (FLSC) (Fig. 6B). According to our measurements, compact FLSC was shown with a periodicity of approximately 100 nm being surrounded by native vitreous collagen (Fig. 6C). Native vitreous collagen fibrils were characterized by regular distribution and a fibril diameter of approximately 16 nm (mean 15.6 nm, SD 2.9 nm; $n = 10$ per image). Strands of native collagen were often found with shortened collagen fibrils at one side of the

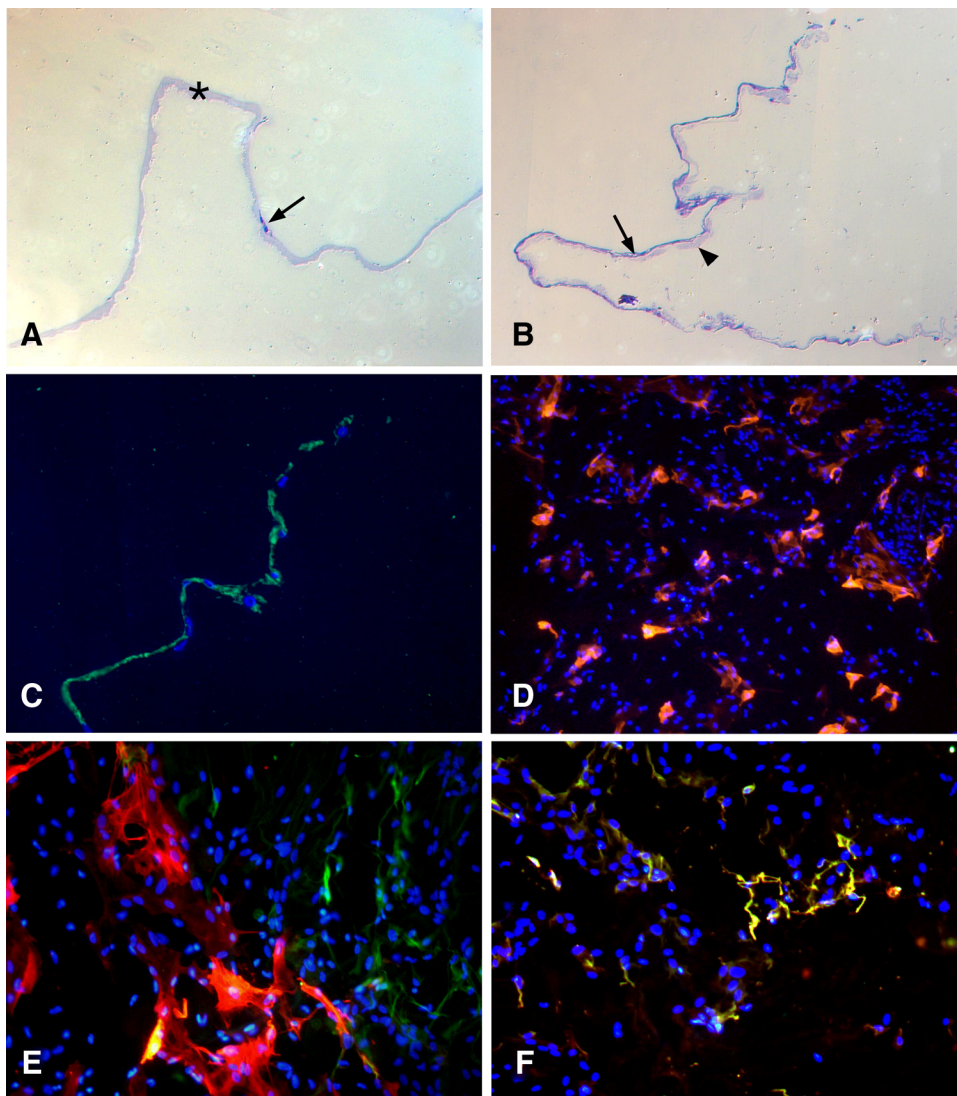


FIGURE 5. Morphologic and immunohistochemical findings of epiretinal tissue with characteristic tractional appearance removed for lamellar macular hole with “tractional” ERM. (A–C) Light micrographs of embedded sections (Lowicryl) with toluidine blue staining. (D–F) Immunofluorescence evaluation of flat-mounted ILM specimens peeled en bloc with epiretinal cell proliferation. (A) ILM (asterisk) with characteristic undulated retinal side and single epiretinal cells (arrow) at the smooth vitreal side. (B) Collagen band (arrowhead) with continuous cell proliferation (arrow). (C) Positive anti-GFAP staining (green) with DAPI cell nuclei staining (blue) of continuous epiretinal cell proliferation. (D) Flat-mounted ILM specimen presents homogeneously distributed cell nuclei (blue) stained by DAPI with positive anti- α -SMA staining (red) characteristic for intracellular actin filaments of myofibroblasts. (E) Merged image of anti- α -SMA (red) and anti-GFAP (green) staining, demonstrating that there was no coexpression of both antigens seen in this series. (F) Merged image presenting colocalization of anti-GFAP and anti-CD45 in epiretinal cells (yellow). Original magnification: (A, B) $\times 200$; (C) $\times 400$; (D) $\times 100$; (E, F) $\times 200$.

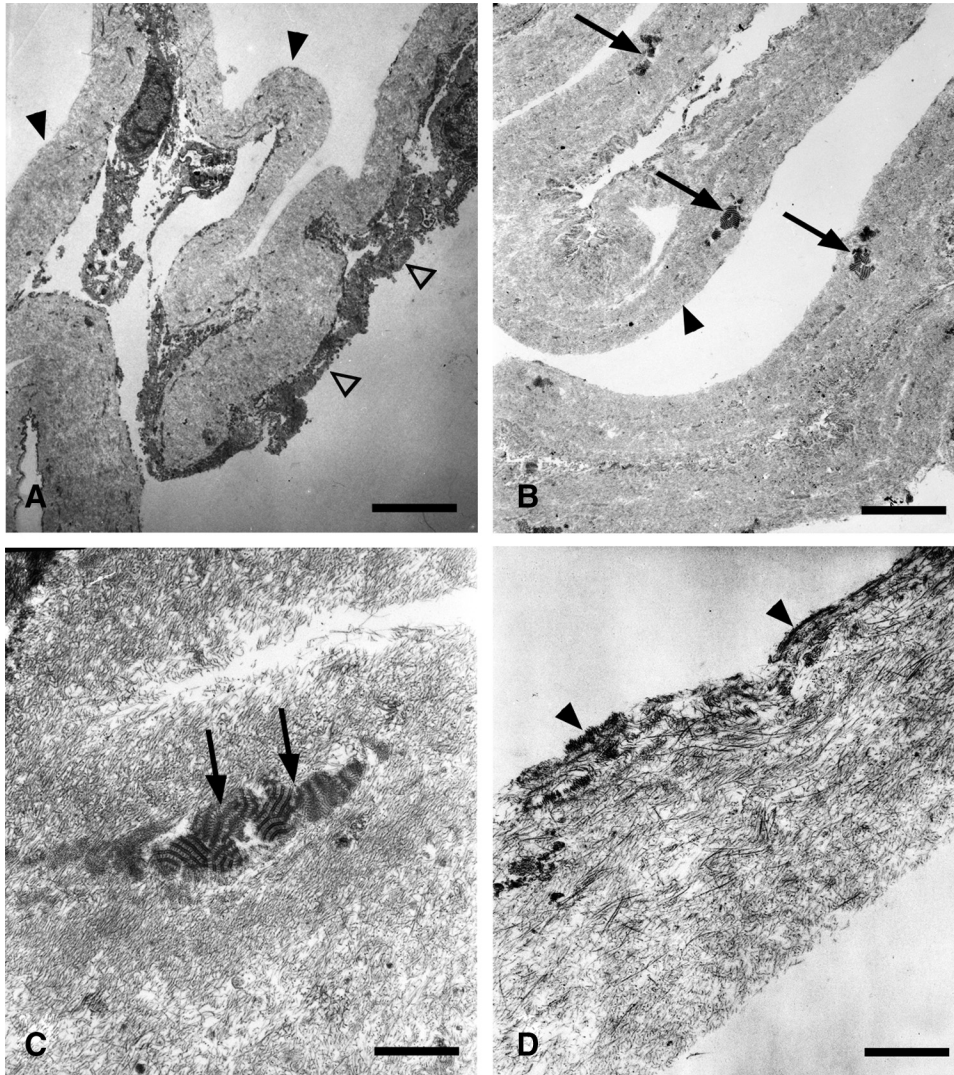


FIGURE 6. Transmission electron micrographs of epiretinal tissue removed from lamellar macular holes with “dense” ERM. **(A)** Tissue composed of masses of collagen bands (*black arrowheads*) with compact undulations and sparse cell proliferation (*white arrowheads*) lacking the ILM. **(B)** Abundant clusters of fibrous long-spacing collagen (*arrow*) were found embedded in collagen bands (*arrowhead*). **(C)** Higher magnification of fibrous long-spacing collagen (*arrow*) embedded in native vitreous collagen fibrils regularly distributed with a mean fibril diameter of 15.6 nm (SD 2.9 nm; $n = 10$). **(D)** Vitreous strand with shortened and compactly sorted collagen fibrils at one side of the strand (*arrowheads*). Original magnification: **(A)** $\times 1800$, bar = 5.6 μm ; **(B)** $\times 4800$, bar = 2.0 μm ; **(C, D)** $\times 9500$, bar = 1.0 μm .

strand (Fig. 6D). These modified native vitreous collagen fibrils were compactly sorted and, therefore, they presented with increased electrodensity.

“Dense” membranes that were found with extrafoveal co-existing tractional epiretinal cell proliferation presented similar to all other “dense” membranes. No morphologic difference could be found.

In “tractional” membranes we found native vitreous collagen fibrils mainly embedded between the ILM and epiretinal cell proliferations (Fig. 7A). The ILM was multiply folded. Epiretinal cell processes presented spanning from one fold to the other. The predominant cell types were fibrous astrocytes and fibroblasts (Fig. 7B). FLSC was less frequently seen in “tractional” membranes compared with “dense” membranes (Fig. 7C), but it was surrounded by native vitreous collagen as well (Fig. 7D).

Cell-type-Specific Antigen Expression

As demonstrated in Table 4, anti-GFAP labeling was found in specimens of all eyes with lamellar macular holes. Anti-GFAP expression was predominant compared with all other antibodies tested. Positive anti-GFAP staining was found irrespective of the group of “dense” or “tractional” membranes (Figs. 4C, 5C). The hyalocyte cell markers CD45 and CD64 were mostly found in both groups as well, although they were sparsely distributed

compared with GFAP (Figs. 4D, 4E). In single specimens, anti-CD45 or anti-CD64 was colocalized with anti-GFAP (Figs. 4F, 5F). Anti-cellular retinaldehyde binding protein (anti-CRALBP) was rarely found. Anti- α -smooth muscle actin (α -SMA) was frequently positive in “tractional” membranes but sparsely distributed in “dense” membranes (Fig. 5D). Anti-GFAP-labeled cells were mostly demonstrated in direct neighborhood to α -SMA-positive cells, but it was never found to be colocalized with anti- α -SMA (Fig. 5E). Anti-CD68 and anti-neurofilament were not demonstrated in this series.

There were proportions of cells in all specimens showing no labeling with any cell marker combination used in this study. In all control specimens, when the primary antibody was substituted by diluent, no immunoreactivity was observed.

CONCLUSIONS

Herein, we present the first clinicopathologic report of LMHs distinguishing between “tractional” ERMs and “dense” ERMs by OCT assessment and intraoperative observation. In contrast to other traction maculopathies with epiretinal membrane formation, we report on attached posterior vitreous cortex in the majority of cases. Epiretinal tissue of both groups presented with characteristic morphologic and immunohistochemical features. There is morphologic evidence of massive vitreous

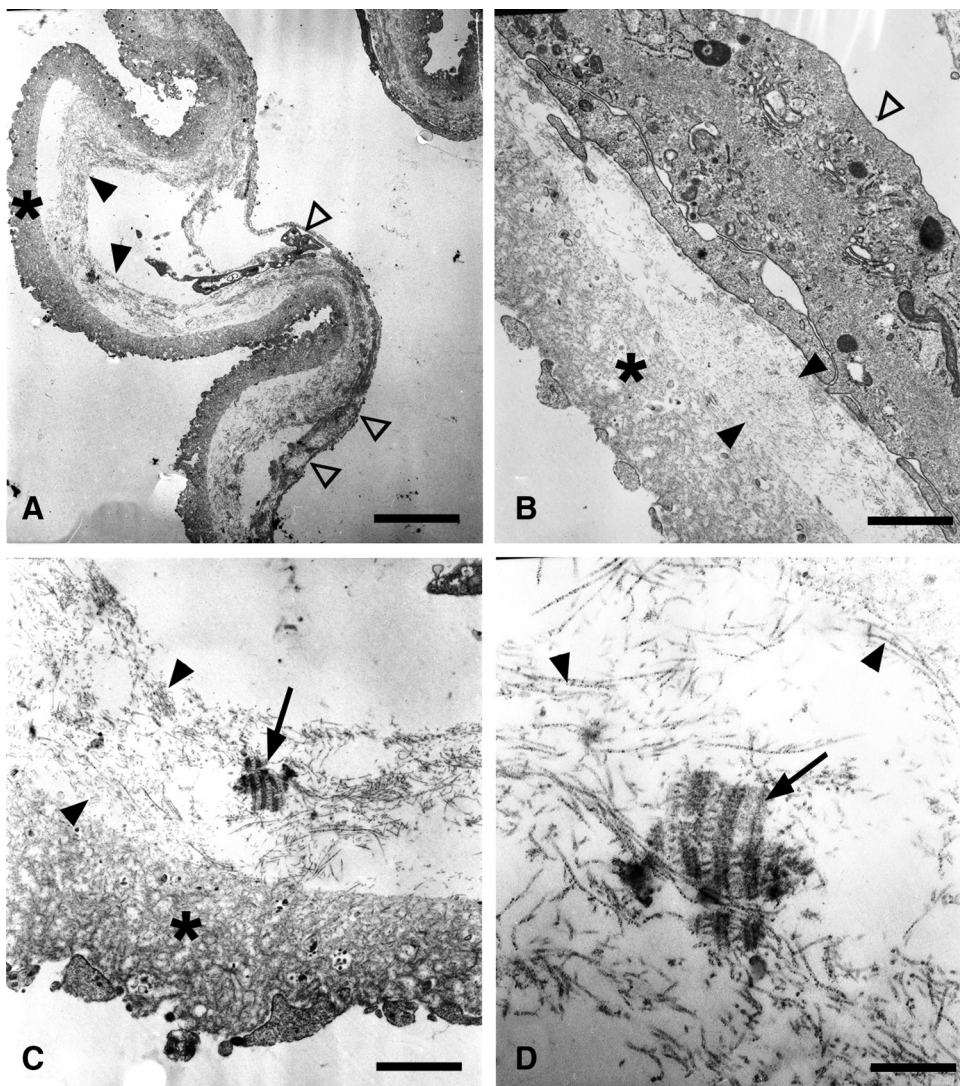


FIGURE 7. Transmission electron micrographs of epiretinal tissue removed from lamellar macular holes with “tractional” ERM. (A) Tissue composed of the multiply folded ILM (*asterisk*), adjacent native vitreous collagen (*arrows*), and epiretinal cell processes that span from one fold to the other (*arrowheads*). (B) Higher magnification of the ILM (*asterisk*) with vitreous collagen fibrils (*arrows*) and epiretinal cells that most probably constitute fibroblasts (*arrowhead*), with prominent Golgi complexes and endoplasmic reticulum. (C) Fibrous long-spacing collagen (*arrow*) embedded in native vitreous collagen fibrils (*arrows*) regularly distributed at the ILM (*asterisk*). (D) Higher magnification of fibrous long-spacing collagen (*arrow*) embedded in single vitreous collagen fibrils of the same detail as (C). Original magnification: (A) $\times 1800$, bar = 5.6 μm ; (B, C) $\times 9500$, bar = 1.0 μm ; (D) $\times 28,500$, bar = 0.4 μm .

collagen degradation that has not been shown before and that may provide new insights into the pathogenesis of LMH by differentiating LMHs from other vitreoretinal disorders such as idiopathic macular holes, macular pucker, and vitreomacular traction syndrome.

In our specimens of “dense” membranes, we found a predominance of native vitreous collagen fibrils by electron microscopic evaluation demonstrating the presence of posterior cortical vitreous. Embedded in native vitreous collagen, only

some newly formed collagen fibrils, but abundant clusters of compact FLSC, were seen. Although FLSC has been reported in tissue from various physiologic and pathologic conditions, including ERMs of macular holes and vitreomacular traction syndrome,^{10,11} it was rarely found in such an abundance as shown in this study. FLSC is a fibrillar precipitate of collagen molecules that is believed to represent an intermediate stage of collagen in the degradation of normal fibrillar collagen.^{12,13} Degradation of collagen might be due to cell-cell and cell-matrix interactions. The presence of FLSC in “dense” and “tractional” membranes in LMHs may represent morphologic evidence for a remodeling process of the premacular cortical vitreous that is supported by the ultrastructural finding of shortened and compact sorted vitreous collagen fibrils in vitreous strands. We hypothesize that structural changes in collagen by cell-cell and cell-matrix interactions may lead to diffusely condensed cortical vitreous. According to the ultra-high-resolution OCT study of Witkin and colleagues,¹ ERMs with “unusual” appearance, comparable to our group of “dense” ERMs, seem to represent thickened and degraded posterior hyaloid with embedded epiretinal cells attached to the macula.

Of note, in the majority of cases we found the posterior vitreous cortex to be attached to the retina intraoperatively. This finding is in contrast to previous data on LMHs¹⁴ and to

TABLE 4. Cell-type-Specific Antigen Expression in Epiretinal Membranes Removed for Lamellar Macular Holes

Anti-	Staining Patterns in	
	“Dense” Membranes	“Tractional” Membranes
GFAP	+	+
CRALBP	(+)	-
NF	-	-
α -SMA	(+)	+
CD45	(+)	(+)
CD64	(+)	+
CD68	-	-

+, positive; (+), sparse; -, negative.

previous reports on the presence of epiretinal cell proliferation in other traction maculopathies.¹⁵⁻¹⁷ However, in the context of attached posterior vitreous cortex, vitreous collagen degradation appears to represent structural changes within the posterior hyaloid that may play an important role in the pathogenesis of LMH. It remains speculative if the remodeling process in attached posterior vitreous rather stabilize retinal anatomy or if it continues to epiretinal fibrocellular proliferation driving contraction. However, the absence of complete or incomplete PVD in LMHs in this study seems to be an important difference to other vitreomacular disorders such as idiopathic macular holes, macular pucker, and vitreomacular traction syndrome.^{10,18-20}

By immunohistochemistry, we found a frequent expression of GFAP in specimens of both groups, “tractional” and “dense” ERMs. The positivity for GFAP in our study is in accordance with previous reports on epiretinal tissue removed for several vitreomacular disorders.^{11,20,21} For decades, GFAP was believed to be typically expressed in glia, and immunolabeling against this intermediate filament protein was thought to be specific to detect astrocytes or pathologic dedifferentiated and migrated retinal Müller cells in epiretinal membranes.²¹⁻²³

In this study, we demonstrate for the first time that the hyalocyte cell markers CD45 and CD64 were occasionally positive tested in colocalization with GFAP in both groups of ERMs removed from eyes with LMHs. Given the colocalization of GFAP and hyalocyte cell markers, we hypothesize that these cells most probably may represent hyalocytes. They may either demonstrate positive GFAP labeling as a result from phagocytic activity of glial cell debris and apoptotic glial cells, or from endogenous expression holding some progenitor potential.

One important difference between “tractional” and “dense” membranes was shown by immunolabeling of α -SMA, the expression of which was more frequently demonstrated in “tractional” ERMs than that in “dense” ERMs. There was no colocalization found with GFAP, but α -SMA-positive cells were shown in direct neighborhood to GFAP-positive cells. α -SMA is an intracellular actin presumed to be essential for extracellular matrix contraction.²⁴ The content of α -SMA in epiretinal membranes was demonstrated to be correlated with clinical contractility.²⁵ Cells of glial origin were shown to lose their typical GFAP expression by undergoing myofibroblast-like transdifferentiation, thereby losing the intermediate filament GFAP with coincident gains of α -SMA immunoreactivity.²⁶ Myofibroblast-like cells were also seen in other vitreomacular disorders such as idiopathic macular hole and vitreomacular traction syndrome.^{18,19} However, contractile elements such as myofibroblast-like cells were not only proposed to originate from glial cells but also from hyalocytes or retinal pigment epithelial cells.^{27,28}

Regarding more frequent positive α -SMA labeling in “tractional” than in “dense” membranes, we postulate that “tractional” membranes possess more potential to generate tractional forces at the retina than “dense” membranes. This hypothesis is supported by clinical findings of our patients diagnosed with “tractional” ERMs in LMHs. Signs of retinal traction, such as retinal folds in biomicroscopy and infrared images, and symptoms of retinal traction, such as metamorphopsia, were demonstrated only in patients with “tractional” membranes. In contrast, patients with “dense” ERMs in LMHs did not show either retinal folding or complaining of metamorphopsia.

At OCT, “dense” and “tractional” membranes look different. In “tractional” membranes a thin hyperreflective line is immediately anterior and separate from the RNFL, whereas in “dense” membranes we observed a thin hyperreflective line in addition to a moderately reflective material filling the space between the inner border of this line and the RNFL. These tomographic findings were similarly observed by Witkin and

colleagues.¹ Correlating retinal imaging with morphologic and immunohistochemical findings, we raise the hypothesis that “tractional” membranes have more potential to generate tractional forces at the retina than “dense” membranes. However, it remains speculative if LMHs with “tractional” ERMs and LMHs with “dense” ERMs constitute different disease entities, or if LMHs with “dense” membranes convert into LMHs with “tractional” membranes over a period representing different stages of one macular disorder.

Surgical intervention in eyes with LMHs still remains controversial. During recent years, several studies reported on a beneficial effect of ERM/ILM peeling in LMHs. However, to our knowledge there is no definite recommendation of surgery that is generally accepted. Thus, mostly vitrectomy with ERM/ILM peeling is recommended in three variable settings: progression of symptoms, such as significant decrease in visual acuity during preoperative follow-up period and/or significant impairment and decrease of quality of daily life; association with a decrease in foveal thickness and/or an increase of LMH diameter in OCT examination; and the presence of ERM and/or complaining of metamorphopsia. In this study, recommendation of surgery was not based on deterioration of BCVA alone. However, with regard to visual acuity, there are reports on statistically relevant functional benefit in cases with preoperative BCVA of 0.4 logMAR or better.¹⁴ Functional benefit after LMH surgery was demonstrated as a mean gain of 2 to 3 Snellen lines in previous studies.^{8,14,29-31} In accordance, we found a mean gain of 2 Snellen lines. Although gain in vision was restricted to a few lines, the improvement of visual acuity was statistically significant in patients with both “dense” and “tractional” membranes. Only five of our patients were found with unchanged vision. All other patients were found with improved visual acuity. None of our patients experienced deterioration of vision.

However, despite frequent improvement of postoperative architecture and recent reports on improvement of visual acuity after vitrectomy with ERM/ILM peeling, there are also data suggesting that surgical intervention may not be helpful.^{32,33} Witkin and colleagues³² reported on four patients after LMH surgery, presenting only one patient with successful anatomic and visual improvement, whereas two other patients developed full-thickness macular holes after vitrectomy. Moreover, several observational case series described LMH as a relatively stable condition.^{34,35} In this study, we found three (15.8%) patients that developed full-thickness macular holes after LMH surgery, thereby requiring additional surgery. Since the progression of LMH to a full-thickness macular hole represents a severe, more notable complication and the improvement of vision appears to be restricted to a limited number of lines, we suggest surgical intervention in patients with LMHs only after careful risk calculation in relation to patients’ symptoms and complaints.

Acknowledgments

The authors thank Renate Scheler, Department of Ophthalmology, Vitreoretinal and Pathology Unit, Ludwig-Maximilians-University, Munich, for assistance in specimen preparation and for her critical comments.

References

1. Witkin AJ, Ko TH, Fujimoto JG, et al. Redefining lamellar holes and the vitreomacular interface: an ultrahigh-resolution optical coherence tomography study. *Ophthalmology*. 2006;113:388-397.
2. Gass JD. Lamellar macular hole: a complication of cystoid macular edema after cataract extraction: a clinicopathologic case report. *Trans Am Ophthalmol Soc*. 1975;73:231-250.

3. Haouchine B, Massin P, Gaudric A. Foveal pseudocyst as the first step in macular hole formation: a prospective study by optical coherence tomography. *Ophthalmology*. 2001;108:15-22.
4. Haouchine B, Massin P, Tadayoni R, et al. Diagnosis of macular pseudoholes and lamellar macular holes by optical coherence tomography. *Am J Ophthalmol*. 2004;138:732-739.
5. Takahashi H, Kishi S. Tomographic features of a lamellar macular hole formation and a lamellar hole that progressed to a full-thickness macular hole. *Am J Ophthalmol*. 2000;130:677-679.
6. Ramirez JA, Karatas M, Fatum S, Halpert M, Ophir A. Lamellar macular hole and continuous vitreofoveal adherence. *Harefuah*. 2005;144:794-797.
7. Ophir A, Fatum S. Cystoid foveal oedema in symptomatic inner lamellar macular holes. *Eye*. 2009;23:1781-1785.
8. Garretson BR, Pollack JS, Ruby AJ, et al. Vitrectomy for a symptomatic lamellar macular hole. *Ophthalmology*. 2008;115:884-886.
9. Schumann RG, Eibl KH, Zhao F, et al. Immunocytochemical and ultrastructural evidence of glial cells and hyalocytes in internal limiting membrane specimens of idiopathic macular holes. *Invest Ophthalmol Vis Sci*. 2011;52:7822-7834.
10. Messmer EM, Heidenkummer HP, Kampik A. Ultrastructure of epiretinal membranes associated with macular holes. *Graefes Arch Clin Exp Ophthalmol*. 1998;236:248-254.
11. Shinoda K, Hirakata A, Hida T, et al. Ultrastructural and immunohistochemical findings in five patients with vitreomacular traction syndrome. *Retina*. 2000;20:289-293.
12. Dingemans KP, Teeling P. Long-spacing collagen and proteoglycans in pathologic tissue. *Ultrastruct Pathol*. 1994;18:539-547.
13. Ishida S, Yamazaki K, Shinoda K, et al. Macular hole retinal detachment in highly myopic eyes. Ultrastructure of surgically removed epiretinal membrane and clinicopathologic correlation. *Retina*. 2000;20:176-183.
14. Androudi S, Stangos A, Brazitikos PD. Lamellar macular holes: tomographic features and surgical outcome. *Am J Ophthalmol*. 2009;148:420-426.
15. Sebag J. Anatomy and pathology of the vitreo-retinal interface. *Eye*. 1992;6:541-552.
16. Johnson MW. Posterior vitreous detachment: evolution and complications of its early stages. *Am J Ophthalmol*. 2010;149:371-382.
17. Sebag J. Anomalous posterior vitreous detachment: a unifying concept in vitreo-retinal disease. *Graefes Arch Clin Exp Ophthalmol*. 2004;242:690-698.
18. Gandorfer A, Rohleder M, Kampik A. Epiretinal pathology of vitreomacular traction syndrome. *Br J Ophthalmol*. 2002;86:902-909.
19. Schumann RG, Schaumberger MM, Rohleder M, et al. Ultrastructure of the vitreomacular interface in full-thickness idiopathic macular holes: a consecutive analysis of 100 cases. *Am J Ophthalmol*. 2006;141:1112-1119.
20. Okada M, Ogino N, Matsumura M, et al. Histological and immunohistochemical study of idiopathic epiretinal membrane. *Ophthalmic Res*. 1995;27:118-128.
21. Hiscott PS, Grierson I, Trombetta CJ, et al. Retinal and epiretinal glia: an immunohistochemical study. *Br J Ophthalmol*. 1984;68:698-707.
22. Bringmann A, Wiedemann P. Involvement of Müller glial cells in epiretinal membrane formation. *Graefes Arch Clin Exp Ophthalmol*. 2009;247:865-883.
23. Middeldorp J, Hol EM. GFAP in health and disease. *Prog Neurobiol*. 2011;93:421-443.
24. Arora PD, McCulloch CA. Dependence of collagen remodeling and α -smooth muscle actin expression by fibroblasts. *J Cell Physiol*. 1994;159:161-175.
25. Sramek SJ, Wallow ICH, Stevens TS, et al. Immunostaining of preretinal membranes for actin, fibronectin, and glial fibrillary acidic protein. *Ophthalmology*. 1989;96:835-841.
26. Guidry C, King JL, Mason JO. Fibrocontractive Müller cell phenotypes in proliferative diabetic retinopathy. *Invest Ophthalmol Vis Sci*. 2009;50:1929-1939.
27. Kohno R-I, Hata Y, Kawahara S, et al. Possible contribution of hyalocytes to idiopathic epiretinal membrane formation and its contraction. *Br J Ophthalmol*. 2009;93:1020-1026.
28. Gamulescu MA, Chen Y, He S, et al. Transforming growth factor β_2 -induced myofibroblastic differentiation of human pigment epithelial cells: regulation by extracellular matrix proteins and hepatocyte growth factor. *Exp Eye Res*. 2006;83:212-222.
29. Michalewski Z, Michalewski J, Odrobina D, et al. Surgical treatment of lamellar macular holes. *Graefes Arch Clin Exp Ophthalmol*. 2010;248:1395-1400.
30. Engler C, Schaal KB, Höh AE, et al. Surgical treatment of lamellar macular hole. *Ophthalmologie*. 2008;105:836-839.
31. Casparis H, Bovey EH. Surgical treatment of lamellar macular hole associated with epimacular membrane. *Retina*. 2011;31:1783-1790.
32. Witkin AJ, Castro LC, Reichel E, et al. Anatomic and visual outcome of vitrectomy for lamellar macular holes. *Ophthalmic Surg Lasers Imaging*. 2010;5:1-7.
33. Kokame GT, Tokuhara KG. Surgical management of inner lamellar macular holes. *Ophthalmic Surg Lasers Imaging*. 2007;38:61-63.
34. Theodossiadis PG, Grigoropoulos VG, Emfietzoglou I, et al. Evolution of lamellar macular hole studies by optical coherence tomography. *Graefes Arch Clin Exp Ophthalmol*. 2009;247:13-20.
35. Tanaka Y, Shimada N, Moriyama M, et al. Natural history of lamellar macular holes in highly myopic eyes. *Am J Ophthalmol*. 2011;152:96-99.